

COSMOS : Hubble Space Telescope Observations

N. Scoville^{1,2}, R. G. Abraham³, H. Aussel^{4,20}, J. E. Barnes⁴, A. Benson¹, A. W. Blain¹, D. Calzetti⁵, A. Comastri³², P. Capak¹, C. Carilli⁶, J. E. Carlstrom⁷, C. M. Carollo⁸, J. Colbert³¹, E. Daddi⁹, R. S. Ellis¹, M. Elvis¹⁰, S. P. Ewald¹, M. Fall⁵, A. Franceschini³⁵, M. Giavalisco⁵, W. Green¹, R. E. Griffiths¹¹, L. Guzzo¹², G. Hasinger¹³, C. Impey¹⁴, J-P. Kneib¹⁵, J. Koda¹, A. Koekemoer⁵, O. Lefevre¹⁵, S. Lilly⁸, C. T. Liu³³, H. J. McCracken^{17,34}, R. Massey¹, Y. Mellier¹⁷, S. Miyazaki¹⁸, B. Mobasher⁵, J. Mould⁹, C. Norman¹⁹, A. Refregier²⁰, A. Renzini^{21,35}, J. Rhodes^{1,22}, M. Rich²³, D. B. Sanders⁴, D. Schiminovich²⁴, E. Schinnerer²⁵, M. Scodreggio³⁸, K. Sheth^{1,31}, P. L. Shopbell¹, Y. Taniguchi²⁶, N. D. Tyson¹⁶, C. M. Urry²⁷, L. Van Waerbeke²⁸, P. Vettolani²⁹, S. D. M. White³⁰, L. Yan³¹, G. Zamorani²⁹

*Based on observations with the NASA/ESA *Hubble Space Telescope*, obtained at the Space Telescope Science Institute, which is operated by AURA Inc, under NASA contract NAS 5-26555.

¹California Institute of Technology, MC 105-24, 1200 East California Boulevard, Pasadena, CA 91125

²Visiting Astronomer, Univ. Hawaii, 2680 Woodlawn Dr., Honolulu, HI, 96822

³Department of Astronomy and Astrophysics, University of Toronto, 60 St. George Street, Room 1403, Toronto, ON M5S 3H8, Canada

⁴Institute for Astronomy, 2680 Woodlawn Dr., University of Hawaii, Honolulu, Hawaii, 96822

⁵Space Telescope Science Institute, 3700 San Martin Drive, Baltimore, MD 21218

⁶National Radio Astronomy Observatory, P.O. Box 0, Socorro, NM 87801-0387

⁷Department of Physics, University of Chicago, 5640 South Ellis Avenue, Chicago, IL 60637

⁸Department of Physics, ETH Zurich, CH-8093 Zurich, Switzerland

⁹National Optical Astronomy Observatory, P.O. Box 26732, Tucson, AZ 85726

¹⁰Harvard-Smithsonian Center for Astrophysics, 60 Garden Street, Cambridge, MA 02138

¹¹Department of Physics, Carnegie Mellon University, 5000 Forbes Avenue, Pittsburgh, PA 15213

¹²Osservatorio Astronomico di Brera, via Brera, Milan, Italy

¹³Max Planck Institut für Extraterrestrische Physik, D-85478 Garching, Germany

¹⁴Steward Observatory, University of Arizona, 933 North Cherry Avenue, Tucson, AZ 85721

¹⁵Laboratoire d'Astrophysique de Marseille, BP 8, Traverse du Siphon, 13376 Marseille Cedex 12, France

¹⁶American Museum of Natural History, Central Park West at 79th Street, New York, NY 10024

¹⁷Institut d'Astrophysique de Paris, UMR7095 CNRS, Université Pierre et Marie Curie, 98 bis Boulevard Arago, 75014 Paris, France

¹⁸Subaru Telescope, National Astronomical Observatory of Japan, 650 North Aohoku Place, Hilo, HI 96720.

¹⁹Department of Physics and Astronomy, Johns Hopkins University, Homewood Campus, Baltimore, MD 21218

²⁰Service d'Astrophysique, CEA/Saclay, 91191 Gif-sur-Yvette, France

²¹European Southern Observatory, Karl-Schwarzschild-Str. 2, D-85748 Garching, Germany

²²Jet Propulsion Laboratory, Pasadena, CA 91109

²³Department of Physics and Astronomy, University of California, Los Angeles, CA 90095

²⁴Department of Astronomy, Columbia University, MC2457, 550 W. 120 St. New York, NY 10027

²⁵Max Planck Institut für Astronomie, Königstuhl 17, Heidelberg, D-69117, Germany

²⁶Physics Department, Graduate School of Science, Ehime University, 2-5 Bunkyo, Matuyama, 790-8577,

ABSTRACT

The Cosmic Evolution Survey (COSMOS) was initiated with an extensive allocation (590 orbits in Cycles 12-13) using the Hubble Space Telescope (HST) for high resolution imaging. Here we review the characteristics of the HST imaging with the Advanced Camera for Surveys (ACS) and parallel observations with NICMOS and WFPC2. A square field (1.8 °) has been imaged with single-orbit ACS I-F814W exposures with 50% completeness for sources $0.5''$ in diameter at $I_{AB} = 26.0$ mag. The ACS imaging is a key part of the COSMOS survey, providing very high sensitivity and high resolution ($0.09''$ FWHM, $0.05''$ pixels) imaging and detecting 1.2 million objects to a limiting magnitude of 26.5 (AB). These images yield resolved morphologies for several hundred thousand galaxies. The small HST PSF also provides greatly enhanced sensitivity for weak lensing investigations of the dark matter distribution.

Subject headings: cosmology: observations — cosmology: large scale structure of universe — cosmology: dark matter — galaxies: formation — galaxies: evolution — surveys

Japan

²⁷Department of Astronomy, Yale University, P.O. Box 208101, New Haven, CT 06520-8101

²⁸Institut d’Astrophysique de Paris, 98 bis, boulevard Arago, F-75014 Paris, France.

²⁹INAF-Osservatorio Astronomico di Bologna, via Ranzani 1, I-40127 Bologna, Italy

³⁰Max-Planck-Institut für Astrophysik, D-85748 Garching bei München, Germany

³¹Spitzer Science Center, California Institute of Technology, Pasadena, CA 91125

³²INAF-Osservatorio Astronomico di Bologna, via Ranzani 1, 40127 Bologna, Italy

³³Astrophysical Observatory, City University of New York, College of Staten Island, 2800 Victory Blvd, Staten Island, NY 10314

³⁴Observatoire de Paris, LERMA, 61 Avenue de l’Observatoire, 75014 Paris, France

³⁵Dipartimento di Astronomia, Universit di Padova, vicolo dell’Osservatorio 2, I-35122 Padua, Italy

³⁶Istituto di Astrofisica Spaziale e Fisica Cosmica, CNR, via Bassini 15, 20133 Milano, Italy

1. Introduction

Sensitive, high resolution imaging is a critical component of all cosmological evolution studies, especially for surveys probing the evolution of luminous galaxies at redshift $z > 0.5$, when most galaxy assembly and evolution occurred. This approach was initiated in HST Treasury surveys : first, the HDFs (Williams et al. 1996, 2000) which imaged a $5 \square'$ area, followed by GOODS (Giavalisco et al. 2004) which covered a larger area ($360 \square'$), GEMS (Rix et al. 2004) which was still more extensive ($800 \square'$) but at shallower depth and, most recently, the UDF survey (Beckwith et al. 2006) which was extremely deep but covered only $11 \square'$. The Cosmic Evolution Survey (COSMOS) with a $2 \square^\circ$ field, is the first HST survey specifically designed to thoroughly probe the evolution of galaxies, AGN and dark matter in the context of their cosmic environment (i.e. large scale structure – LSS). COSMOS samples all relevant scales of LSS – up to $\sim 50 - 100 h_{70}^{-1}$ Mpc at all $z > 0.5$. The area of COSMOS was designed to sample the full dynamic range of large scale structures from voids to very massive clusters. (HST-ACS coverage of the DEEP Groth strip covers $\sim 10 \times 70'$ Faber et al. (2006), similar to GEMS, but the elongated geometry is not optimum for sampling the larger structures.) High resolution imaging with HST enables accurate determination of galaxy morphologies and multiplicities. The HST imaging also provides significantly improved weak lensing analysis to probe the dark matter distribution of the LSS.

COSMOS is the largest HST survey ever undertaken – imaging an equatorial field with single-orbit I-band exposures to a depth $I_{AB} = \sim 28$ mag (5σ on an optimally extracted point source) and 50% completeness for sources $0.5''$ in diameter at $I_{AB} = 26.0$ mag. With this area coverage, COSMOS HST and ground-based imaging detects $\simeq 2 \times 10^6$ objects and samples a volume in the high redshift universe approaching that sampled locally by the Sloan Digital Sky Survey (SDSS). In this article we describe the observations which make up the HST component of the COSMOS survey: the primary ACS imaging and the parallel NICMOS and WFPC2 imaging. A detailed description of the HST data processing is provided in Koekemoer et al. (2006).

2. HST Observations

The original HST Cycle 12 COSMOS proposal had two major components for imaging with the Advanced Camera for Surveys (ACS) : 1) a complete mosaic of $2 \square^\circ$ in the F814W (I-band) filter for morphological information and 2) a similar mosaic in F475W (g-band) to provide resolved color imaging for studies of stellar populations and dust obscuration. Although 640 orbits were allocated for the I-band imaging, 50 orbits were specified to enable searches for SNIa. Following discussions with the principal investigators for the supernova

programs (A. Reiss & S. Perlmutter), the COSMOS team decided that the SNIa science was not easily served within the COSMOS survey strategy, and the 50 orbits were given over to follow-on exposures in the GOODS-S survey field. Thus the COSMOS HST survey (590 orbits total) comprises 270 and 320 orbits allocated within HST Cycles 12 & 13 (Fall 2003 to Spring 2005), respectively.

2.1. Field Selection

Multi-wavelength imaging and optical spectroscopy are central to the ability of the COSMOS survey to probe the evolution of stellar populations, star formation, galaxies and AGN. The enormous investments in observing time, required to cover a $2\Omega^\circ$ field, rule against having separate northern and southern hemisphere fields, as in earlier, smaller surveys. Thus an initial prerequisite for COSMOS was that the field be accessible to telescopes in both hemispheres and especially all unique facilities. This precluded using COSMOS to extend the area of earlier survey fields at high northern or southern Declination (such as HDF-N/S, GOODS/CDF-N/S, Lockman Hole and the Groth strip). An equatorial field is required to enable access by all existing 8-10m optical telescopes (and future larger telescopes) and the unique radio facilities (the (E)VLA in the north and ALMA in the south). ALMA is likely to become a 'required' facility for studies of early universe galaxy evolution; at the same time, high sensitivity VLA radio imaging is critical and the instrument is unique in terms of sensitivity (with a factor of 3-10 improvement for EVLA).

The original field proposed for the COSMOS survey was the VVDS/XMM Deep field centered at $RA = 2^{\text{h}}:26^{\text{m}}$, $DEC = -4.5^\circ$ which was scheduled for extensive optical spectroscopy with the VLT-VIMOS spectrograph. However, during the Phase 2 preparation for COSMOS-HST in Cycle 12 it became apparent that HST was very overcommitted at $RA \sim 2$ hr due to the Ultra-Deep Field (UDF) Directors Discretionary Time project in Cycle 12 – we were therefore requested by both the STScI and ESO directors to consider shifting the COSMOS survey field to a non-conflicting RA. Our examination of alternative equatorial fields, revealed a field near the VVDS 10 hr field which in fact had slightly lower extinction ($E_{B-V} \simeq 0.02$ mag) and far-infrared, cirrus backgrounds (Scoville et al. 2006a) than the original 2 hr VVDS/XMM Deep field. This field also has no extremely bright X-ray, UV, optical and radio sources, unlike some other fields. Since the 10 hr field did not have as extensive prior observational coverage as the 2 hr field, most of the ground-based optical/ir imaging would have to be done as part of COSMOS. However, this enables the COSMOS survey to efficiently observe the entire field to uniform sensitivity and to the optimum depth determined by the COSMOS science.

In conclusion, the final field selected for COSMOS is a $1.4^\circ \times 1.4^\circ$ square, aligned E-W, N-S, centered at RA = $10^h:00^m:28.6^s$, DEC = $+02^\circ:12':21.0''$ (J2000). It has *low and exceptionally uniform optical extinction* (less than 20% variation, see Sanders et al. 2006). Being equatorial, the field has somewhat higher far infrared background than the very best fields such as Lockman Hole (Scoville et al. 2006a); however, this is clearly less detrimental to the overall survey than the penalty of very poor (or nonexistent) radio and mm/submm coverage of higher declination fields by the VLA or ALMA.

A summary of the HST observations is provided in Table 1; below, we briefly discuss each instrument in detail.

2.2. ACS Observations and Processing

Imaging with ACS in the F814W (I-band) filter is the primary COSMOS HST observation. The ACS-WFC field of view (FOV) is $203'' \times 203''$, covered by two CCD arrays separated by a gap of $4.5''$. The pixel size is $0.05''$. Nine of the allocated orbits were devoted to a test 3×3 pointing mosaic in the F475W (g-band) filter at the center of the field in order to evaluate the need for full field coverage in a second filter. Thus a total of 581 orbits/pointings were devoted to imaging in the I-band filter. Within each orbit, four equal length exposures of 507 sec duration each (2028 sec total) were obtained in a 4 position dither pattern, designed to shift bad pixels and to fill in the 90 pixel gap between the two ACS CCD arrays (see Koekemoer et al. 2006). Adjacent pointings in the mosaic were positioned with approximately 4% overlap in order to provide at least 3 exposure coverage at the edge of each pointing and 4 exposure coverage over approximately 95% of the survey area. This multiple exposure coverage with ACS provides excellent cosmic ray rejection (Koekemoer et al. 2006).

The visibility windows for the COSMOS program were set such that two approximately 180° -opposed orientation angles could be scheduled (PA = $290 \pm 10^\circ$ and $110 \pm 10^\circ$ corresponding to 13 October to 7 January and 2 March to 21 May, respectively). (In the HST 2-gyro mode, only the former is available.) Three of the pointings had large reflections or scattered light due to bright stars being on the edge of the ACS FOV. These three fields were later repeated with two exposures placing the bright stars well *within* the ACS FOV. (They are included in the 581 orbit count mentioned above.)

A full description of the ACS data processing including drizzling, flux calibration, registration and mosaicing is provided in Koekemoer et al. (2006). The registration was tied into ground based CFHT i-band imaging (Aussel et al. 2006) with the USNO-B 1.0 reference frame offsets established from the COSMOS VLA survey (Schinnerer et al. 2006). The

absolute registration of all ACS data in the COSMOS archive is accurate to approximately 0.05-0.10'' over the entire field (Koekemoer et al. 2006). The flux calibration of the ACS is tied into the standard STScI ACS calibration, accurate to better than 0.05% in absolute zero point. For the public-released images with 0.05'' pixels, the DRIZZLE parameters (Fruchter & Hook 2002) were : pixfrac = 0.8 and a square kernel was used. For the images used for weak lensing analysis, 0.03'' pixels, pixfrac = 0.8, were used with a Gaussian kernel. (CTE effects on the faint source PSFs were reduced as described in Rhodes et al. (2006).) The final ACS mosaic image released to the public IRSA and MAST archives is sampled with 0.05'' pixels. The measured FWHM of the PSF in the ACS I-band filter is 0.09''. These individual images were also rotated to North up for the public release data. For the purpose of the weak lensing analysis done by the COSMOS team an internal release of the unrotated images, sampled to 0.03'' pixels, was also generated to avoid rotating the original PSF and to reduce aliasing problems associated with resampling (Rhodes et al. 2006); for general morphological studies the rotated and the 0.05'' are entirely adequate.

2.3. NICMOS and WFPC2 Parallel Observations

In parallel with the ACS observations, imaging was obtained with the NICMOS and WFPC2 cameras. WFPC2 was used in coordinated-parallel mode, implying that exposures were obtained with every ACS pointing. The WFPC2 FOV is 150'', offset in position from the ACS field center by 5.8'. Since NICMOS cannot be used in periods of high particle flux such as the SAA passages, the NICMOS observations were set up in pure-parallel mode so as not to impede scheduling of the primary ACS observations. Therefore, not every orbit has an associated NICMOS parallel observation. The NICMOS Camera 3, used for COSMOS parallel observations, has a FOV of 50'' and the field center is displaced 8.5' from that of ACS.

For WFPC2, the filter used initially was F300W. However inspection of the Cycle 12 data revealed a very low rate of object detection at 3000Å; in the second half of Cycle 13, the WFPC2 filter was therefore changed to F450W. The NICMOS parallels used the F160W (1.6μm, H-band) filter. There were 4 and 3 exposures per orbit for WFPC2 and NICMOS, respectively. The WFPC2 and NICMOS parallels cover approximately 55% (1.07 □°) and 6% (0.092 □°, 330 □') of the COSMOS 1.8□° field imaged with ACS. The total areal coverage in NICMOS parallel imaging is probably the largest of any HST project – although it is not contiguous, it provides enormous samples of objects. The details of reduction and calibration of the WFPC2 (done by S. Ewald) and NICMOS (done by J. Colbert) imaging are included in Koekemoer et al. (2006).

3. Sensitivity, Resolution and Coverage

The sensitivities and resolutions for the COSMOS-HST imaging are summarized in Table 2 and compared with those of other HST surveys in Table 3. In order to facilitate direct comparison of the different surveys, we have used the instrument exposure time calculators (ETCs) provided by STScI, rather than published sensitivities of the surveys which were derived with differing assumptions. For ACS and WFPC2, the flux is normalized in the V band; for NICMOS, the flux is normalized to $1.6\mu\text{m}$. (The V-band normalization was adopted to be consistent with Table 3 where the other HST surveys which cover several bands are summarized.) Normalization of the flux to I-band reduces the ACS magnitudes by 1.4 mag (e.g. $28.6 \rightarrow 27.2$ mag). The COSMOS ACS I-band coverage is shown in Figure 1. The rectangle bounding all the ACS imaging has lower left and upper right corners (RA,DEC J2000) at $(150.7988^\circ, 1.5676^\circ)$ and $(149.4305^\circ, 2.8937^\circ)$. The positions observed in the NICMOS parallel observations are shown in Figure 2; the locations of the WFPC2 parallels are not shown given in view of their low sensitivity (see below).

4. Photometric Catalogs

The primary reference catalogs for COSMOS have objects selected from both the ACS images and the very deep, multi-band Subaru-SCAM COSMOS imaging (Taniguchi et al. 2006). The SCAM data are of similar depth to the ACS imaging (approximately 0.8 mag deeper for sources $> 1''$ in diameter but for sources smaller than $\sim 0.3''$, the ACS data are more sensitive). The ground-based imaging (Capak et al. 2006) presently includes 18 filters including narrow and intermediate bandwidth filters. Catalogs were made from both the ACS and Subaru I-band and NICMOS H-band imaging. The ACS catalog comprises 1.2 million objects ((Leauthaud et al. 2006); the NICMOS catalog has 21639 objects ($> 1.5\sigma$ for 9 adjacent pixels). For the ACS catalog, SExtractor (Bertin & Arnouts 1996) was used with the requirement of $> 0.4\sigma$ in at least 4 adjacent pixels and the total isophotal signal-to-noise ratio > 1 . The ACS catalog includes additional internal sub-structures within sources listed in the lower-resolution, ground-based catalog. These catalogs and the derived photometric redshifts (Mobasher et al. 2006) are presented and described in detail elsewhere (Koekemoer et al. 2006; Capak et al. 2006; Leauthaud et al. 2006).

5. Public Data Release

The COSMOS HST data are publicly available in staged releases (following calibration and validation) through the web sites for IPAC/IRSA : <http://irsa.ipac.caltech.edu/data/COSMOS/> and STScI-MAST : <http://archive.stsci.edu/>. (The STScI pipeline processed images are of course also available in the STScI archive.) The COSMOS ACS imaging is in the form of separate drizzled images for each pointing, rotated and resampled to have North up with pixel scale $0.05''$. IRSA also supplies a cutout capability derived from the full field mosaic (50 GB). The cutouts can be made with any field center and size; and multiple cutouts are provided based on a user-supplied file containing source positions and field sizes. The SExtractor catalogs for ACS and NICMOS (see section 4) are also available through IRSA.

6. Source Counts and Completeness

Figures 4 and 5 show the magnitude distributions of sources in the ACS and NICMOS source catalogs (Section 4). The ACS source counts are listed in Table 4. We have compared the ACS I-band source counts with those published by Ferguson et al. (2000) for HDF. In HDF, the derived I-band count at $I_{AB} = 25$ mag is 1.0×10^5 galaxies per square degree per $\Delta m = 1$ mag. For the COSMOS ACS catalog the count is $\sim 21,000$ for 1.8 square degrees per $\Delta m = 0.1$ mag (at $I_{AB} = 25$ mag, see Figure 4). The COSMOS counts are $\sim 16\%$ higher than those in the HDFs, but given the fact that different SExtraction parameters were probably used in COSMOS and HDF the agreement is quite acceptable. The H-band integrated number counts are equivalent to 3478, 14130 and 41300 deg^{-2} per 0.5 mag bin at $H = 20, 22$ and 24 mag (AB). A recent compilation of previous surveys by Frith et al. (2000) has approximately 3300, 15000 and 41000 deg^{-2} in the same bins (see dashed curve in their Figure 1).

The completeness of the ACS catalog was determined using the standard technique of inserting false sources of specified half-light size and total flux (Giavalisco et al. 2004). Size and flux must both be explored since the ability to detect sources depends on their surface brightness and hence their flux and size. The simulated galaxies were a 50/50 mix of exponential disks and $r^{1/4}$ spheroids (Giavalisco et al. 2004). Figure 6 shows contours for the percentage of the test galaxies recovered. For galaxies with half-light radii of 0.25, 0.5 and $1''$, the completeness is $\sim 50\%$ at $I_{AB} \simeq 26.0, 24.7$ and 24.5 mag.

7. Analysis Enabled by COSMOS ACS Observations

The high resolution ACS imaging is critical to the COSMOS survey, providing: galaxy morphologies, multiplicities and merger rates out to $z \geq 2$, environmental density from DM maps at $z \leq 1$, and size and limited morphological information at redshifts out to $z = 6$. The morphological parameters obtained from the ACS imaging include bulge/disk ratios, concentration, asymmetry, size, multiplicity, color, clumpiness (see Cassata et al. (2006); Scarlatta et al. (2006); Capak et al. (2006)). The COSMOS I-band ACS images have sufficient depth and resolution to allow classical bulge-disk decomposition for L^* galaxies at $z \leq 2$, while less detailed structural parameters such as concentration, asymmetry, clumpiness and size can be measured for all galaxies down to the COSMOS spectroscopic survey limit (37,500 galaxies with $I_{AB} \leq 25$; Lilly et al. (2006); Impey et al. (2006)), out to $z \sim 5$. COSMOS ACS imaging has been crucial for the identification and analysis of galactic interactions and mergers (e.g. Kartalepe, Sanders & Scoville (2006)) – processes which are central to the early evolution of galaxies.

For the purposes of weak lensing analysis, approximately 87 galaxies per \square' were sufficiently resolved with ACS (c.f. $\sim 30 \square'$ from Subaru-SCAM). Their median (mean) redshift is 1.02 (1.25), and their per-component rms shear is 0.309. This permits mass reconstructions with an optimal resolution on the sky at scales $\sim 100''$, and a redshift sensitivity that peaks between $z = 0.2$ and $z = 0.6$. These parameters enable detection of $\sim 7 \times 10^{13} M_{\odot}$ cluster at $z = 0.2$ with 5σ signal-to-noise ratio (Rhodes et al. 2006; Massey et al. 2006).

The HST COSMOS Treasury program was supported through NASA grant HST-GO-09822. We wish to thank Tony Roman, Denise Taylor, and David Soderblom for their assistance in planning and scheduling of the extensive COSMOS observations. We gratefully acknowledge the contributions of the entire COSMOS collaboration consisting of more than 70 scientists. More information on the COSMOS survey is available at [http://www.astro.caltech.edu/~sim\\$cosmos](http://www.astro.caltech.edu/~sim$cosmos). It is a pleasure to acknowledge the excellent services provided by the NASA IPAC/IRSA staff (Anastasia Laity, Anastasia Alexov, Bruce Berriman and John Good) in providing online archive and server capabilities for the COSMOS datasets. The COSMOS Science meeting in May 2005 was supported in part by the NSF through grant OISE-0456439. We thank Rob Kennicutt for suggestions on the manuscript.

Facilities: HST (ACS), HST (NICMOS), HST (WFPC2).

REFERENCES

- Aussel, H. et al. 2006, ApJS, this volume.
- Beckwith, S. V. B. et al. 2006 (in preparation).
- Bertin, E. & Arnouts, S. 1996, A&AS, 117, 393.
- Capak, P. et al. 2006, ApJS, this volume.
- Cassata, P., Guzzo, L., Franceschini, A., Scoville, N., Capak, P., Ellis, R. S., Koekemoer, A., McCracken, H. J., Mobasher, B., Scodreggio, M., Taniguchi, Y. & Thompson, D. T. 2006, ApJS, this volume
- Faber, S. et al. 2006, (in preparation).
- Ferguson, H., Dickinson, M. & Williams, R. et al. 2000, ARA&A, 38, 667.
- Frith, W. J., Metcalfe, N. & Shanks, T. et al. 2005, astro-ph/059875.
- Fruchter, A. S. & Hook, R. N. 2002, PASP, 114, 144.
- Giavalisco, M., Ferguson, H. C., Koekemoer, A. M., Dickinson, M., Alexander, D. M., Bauer, F. E., Bergeron, J., Biagetti, C., Brandt, W. N., Casertano, S., Cesarsky, C., Chatzichristou, E., Conselice, C., Cristiani, S., Da Costa, L., Dahlen, T., de Mello, D., Eisenhardt, P., Erben, T., Fall, S. M., Fassnacht, C., Fosbury, R., Fruchter, A., Gardner, J. P., Grogin, N., Hook, R. N., Hornschemeier, A. E., Idzi, R., Jogee, S., Kretchmer, C., Laidler, V., Lee, K. S., Livio, M., Lucas, R., Madau, P., Mobasher, B., Moustakas, L. A., Nonino, M., Padovani, P., Papovich, C., Park, Y., Ravindranath, S., Renzini, A., Richardson, M., Riess, A., Rosati, P., Schirmer, M., Schreier, E., Somerville, R. S., Spinrad, H., Stern, D., Stiavelli, M., Strolger, L., Urry, C. M., Vandame, B., Williams, R. & Wolf, C. 2004, ApJ, 600, 99.
- Kartalepe, J., Sanders, D. S. & Scoville, N. Z. 2006, ApJS, this volume.
- Koekemoer, A. et al. 2006, ApJS, this volume.
- Leauthaud, A. et al. 2006, ApJS, this volume.
- Impey, C. D., Trump, J. R., McCarthy, P. J., Elvis, M., Huchra, J. P., Scoville, N. Z., Lilly, S. J., Brusa, M., Hasinger, G., Schinnerer, E. & Capak, P. 2006, ApJS, this volume.

- Leauthaud, A., Kneib, J-P., Massey, R., Tasca, L., Rhodes, J., Capak, P., Ellis, R., Heymans, C., Koekemoer, A., Le Fevre, O., Mellier, Y., Refregier, A., Robin, A., Scoville, N., Taylor, J., van Waerbeke, L. 2006, ApJS, this volume.
- Lilly, S.J., Le Fvre, O., Renzini, A., Zamorani, G., Scodreggio, M., Contini, T., Carollo, C. M., Hasinger, G., Kneib, J-P, Iovino, A., Le Brun, V., Maier, C. H., Mainieri, V., Mignoli, M. , Silverman, J., Tasca, L., Bolzonella, M., Bongiorno, A., Bottini, D., Capak, P., Cimatti, A., Cucciati, O., Daddi, E., Feldmann, R., Franzetti, P., Garilli, B., Guzzo, L., Ilbert, O., Kampczyk, P., Lamareille, F., Leauthaud, A., Leborgne, J-F, McCracken, H. , Pello, R., Riccardelli, E., Scarlata, C., Vergani, D., Sanders, D., Schinnerer, E., Scoville, N., Taniguchi, Y., Arnouts, S., Aussel, H., Bardelli, S., Brusa, M., Cappi, A., Ciliegi, P., Figuenov, A., Foucaud, S., Franchesini, R., Halliday, C., Impey, C., Knobel, C., Kurk, J., Maccagni, D., Maddox, S., Marano, B., Marconi, G., Marinoni, C., Mobasher, B., Moreau, C., Peacock, J., Porciani, C., Pozetti, L., Scaramella, R., Schminovich, D., Smail, I., Tresse, L., Vettolani, P., Zanichelli, A., & Zucca, E 2006, ApJS, this volume.
- Massey, R. J. et al. 2006, ApJS, this volume.
- Mobasher, B., Capak, P. , Scoville, N. Z. ,Dahlen, T., Salvato, M., Aussel, H., Thompson, D. J., Feldmann, R., Tasca, L., Lefevre, O., Lilly, S.,Carollo, C. M., Kartaltepe, J. S., McCracken, H., Mould, J., Renzini, A.,Sanders, D. B., Shopbell, P. L., Taniguchi, Y., Ajiki, M., Shioya, Y.,Contini, T., Giavalisco, M., Ilbert, O.,Iovino, A., Le Brun, V., Mainieri, V., Mignoli, M., & Scodreggio, M. 2006, ApJS, this volume.
- Rix, H-W, Barden, M. , Beckwith, S. V. B., Bell, E. F. , Borch, A. ,Caldwell, J. A. R. ,Haussler, B., Jahnke, K. , Jogee, S., McIntosh, D. H., Meisenheimer, K., Peng, C. Y., Sanchez, S. F. , Somerville, R. S., Wisotzki, L., & Wolf, C. 2004, ApJS, 152, 163.
- Rhodes, J. R. et al. 2006, ApJS, this volume.
- Sanders, D. B.. et al.2006, ApJS, this volume
- Scarlatta, C. , Carollo, C.M. , Lilly, S.J. , Feldmann, R., Kampczyk, P., Renzini, A., Cimatti, A. , Halliday, C. , Daddi, E., Sargent, M. T. , Koekemoer, A. , Scoville, N. , Kneib, J-P. , Leauthaud, A. , Massey, R. , Rhodes, J. , Tasca, L. , Capak, P. , McCracken, H. J. , Mobasher, B. ,Taniguchi, Y., Thompson, D. J., Ajiki, M. , Aussel, H., Murayama, T., Sanders, D. B., Sasaki, S., Shioya, Y. , Takahashi, M. 2006, ApJS, this volume
- Schinnerer, E. E., Smolcic, V. , Carilli, C. L. , Bondi, M. , Ciliegi, P. , Jahnke, K. , Scoville, N. Z., Bertoldi, F. , Blain, A. W. , Impey, C. D. , Koekemoer, A. M. , Le Fevre, O. , Urry, C. M. & Vettolani, G. 2006, ApJS, this volume.

Scoville, N. Z., Aussel, H., Brusa, M., Capak, P., Carollo, C. M., Elvis, M., Giavalisco, M., Guzzo, L., Hasinger, G., Impey, C. D., Kneib, J-P., LeFevre, O., Lilly, S. J., Mobasher, B., Renzini, A., Rich, R. M., Sanders, D. B., Schinnerer, E., Schminovich, D., Shopbell, P.L., Taniguchi, Y., Tyson, N. D. 2006a, ApJS, this volume.

Taniguchi, Y. et al. 2006, ApJS, this volume.

Williams, R.E., Blacker, B., Dickinson, M., Dixon, W.V., Ferguson, H.C., Fruchter, A.S., Giavalisco, M., Gilliland, R.L., Heyer, I., Katsanis, R., Levay, Z., Lucas, R.A., McElroy, D.B., Petro, L., Postman, M., Adorf, H-M., Hook, R. 1996, AJ, 112, 1335.

Williams, R.E et al. 2000, AJ, 120, 2735.

Table 1. HST Observations

Instrument	Filter	Mode ^a	Orbits	Exposure (sec)	Dates	Proposal ID
ACS	F814W (I-band)	P	261	2028	10/15/03 → 5/21/04	09822 (Cy 12)
ACS	F475W (g-band)	P	9	2028	10/15/03 → 5/21/04	09822 (Cy 12)
ACS	F814W (I-band)	P	320	2028	10/15/04 → 5/21/05	10092 (Cy 13)
NICMOS-NIC3	F160W (H-band)	PP	225	1536	10/15/03 → 5/21/04	09999 (Cy 12)
NICMOS-NIC3	F160W (H-band)	PP	282	1536	10/15/04 → 5/21/05	10337 (Cy 13)
WFPC2	F300W (U-band)	CP	270	1600	10/15/03 → 5/21/04	09822 (Cy 12)
WFPC2	F300W (U-band)	CP	149	1600	10/15/04 → 11/21/04	10092 (Cy 13)
WFPC2	F450W (B-band)	CP	171	1600	11/21/04 → 5/21/05	10092 (Cy 13)

^aScheduling Mode : P – primary, PP – pure-parallel, CP – coordinated-parallel.

Table 2. COSMOS HST Sensitiivities and Resolution

Instrument	Filter	$5\sigma_{AB}$ ^a	$5\sigma_{STmag}$	$5\sigma_{Vega}$	Res(FWHM)	Pixel
ACS	F814W (I-band)	28.6	29.5	28.2	0.09''	0.05''
ACS	F475W (g-band)	27.9	27.6	28.0	0.05''	0.05''
NICMOS-NIC3	F160W (H-band)	25.9	28.3	24.6	0.16''	0.20''
WFPC2	F300W (U-band)	24.8	26.1	24.8	0.10''	0.1(0.046,PC)''
WFPC2	F450W (B-band)	26.7	26.3	26.8	0.10''	0.1(0.046,PC)''

^aSensitivities for optimally-extracted point sources with a λ^{-1} power law spectrum for ACS and NICMOS. For WFPC2, assumes an A0 star spectrum. For ACS and WFPC2, the flux is normalized to V, for NICMOS the flux is normalized to 1.6 μ m. The V-band normalization was adopted to be consistent with Table 3 where surveys in several bands are compared. Normalization of the flux to I-band reduces the ACS magnitudes by 1.4 mag (e.g. 28.6 → 27.2).

Table 3. Relative Pt. Source Sensitivities

Filter	Survey	5σ AB ^a	Orbits	Vega - AB	STmag - AB
F435	UDF	29.94	56	0.11	0.52
..	GOODS	28.32	3
F606	UDF	30.84	56	0.09	0.17
..	GOODS	29.14	2.5
F775	UDF	31.30	150	-0.40	0.74
..	GOODS	29.04	2.5
F814	COSMOS	28.63	1	-0.44	0.84
F850	GOODS	29.11	5	-0.54	1.09
..	UDF	30.99	150

Note. — HDF : Williams et al. (1996, 2000); GOODS : Giavalisco et al. (2004) ; UDF : Beckwith et al. (2006) . To facilitate direct comparison of the different surveys, we have used the instrument exposure time calculators (ETCs) provided by STScI, rather than published sensitivities of the surveys (which were derived with differing assumptions).

^aSensitivities for optimally-extracted point sources; for a source uniformly extended over $\sim 0.25''$ diameter, the limiting magnitudes are ~ 1 mag greater. (Assumes: 2028s per orbit for COSMOS and 2500s per orbit for the other surveys, a λ^{-1} power law spectrum with normalization at V, 4 cr-split/orbit for COSMOS, 2 cr-split/orbit for GOODS and UDF, no reddening)

Table 4. ACS Source Counts

I < mag	all objects	non-stellar
25	288,657	266,039
26	567,143	531,982
27	1,029,007	878,445

Note. — Source counts in F814W ACS images obtained using SExtractor as described in text. The ACS catalog used for lensing studies is present in (Leauthaud et al. 2006).

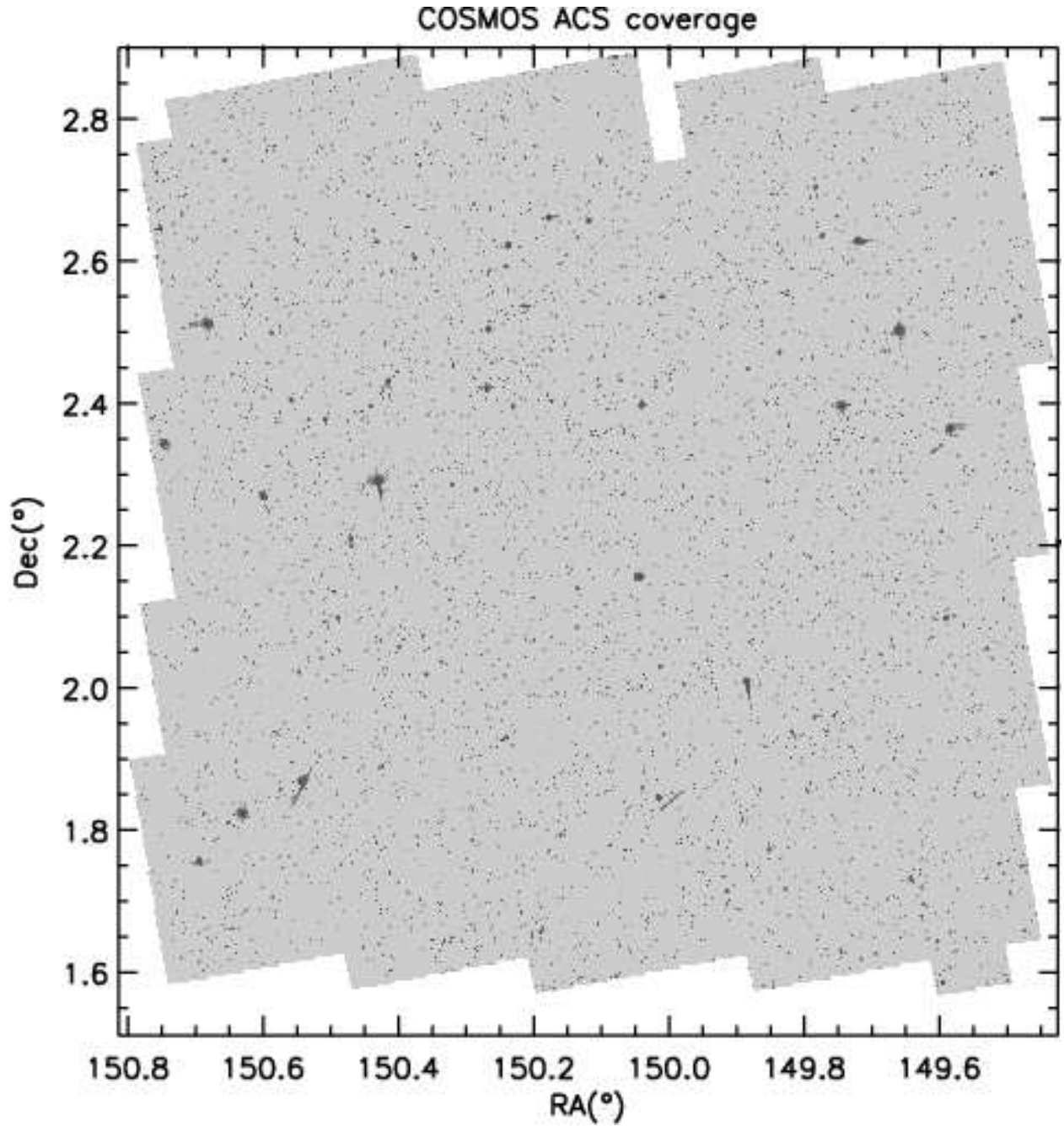


Fig. 1.— The layout of the ACS mosaic of 581 I-band pointings is shown. The rectangle fully enclosing all the ACS imaging has lower left and upper right corners (RA,DEC J2000) at $(150.7988^{\circ}, 1.5676^{\circ})$ and $(149.4305^{\circ}, 2.8937^{\circ})$. The WFPC2 (3000 & 4500Å) and NICMOS ($1.6\mu\text{m}$) images cover approximately 55% and 6% of the ACS area.

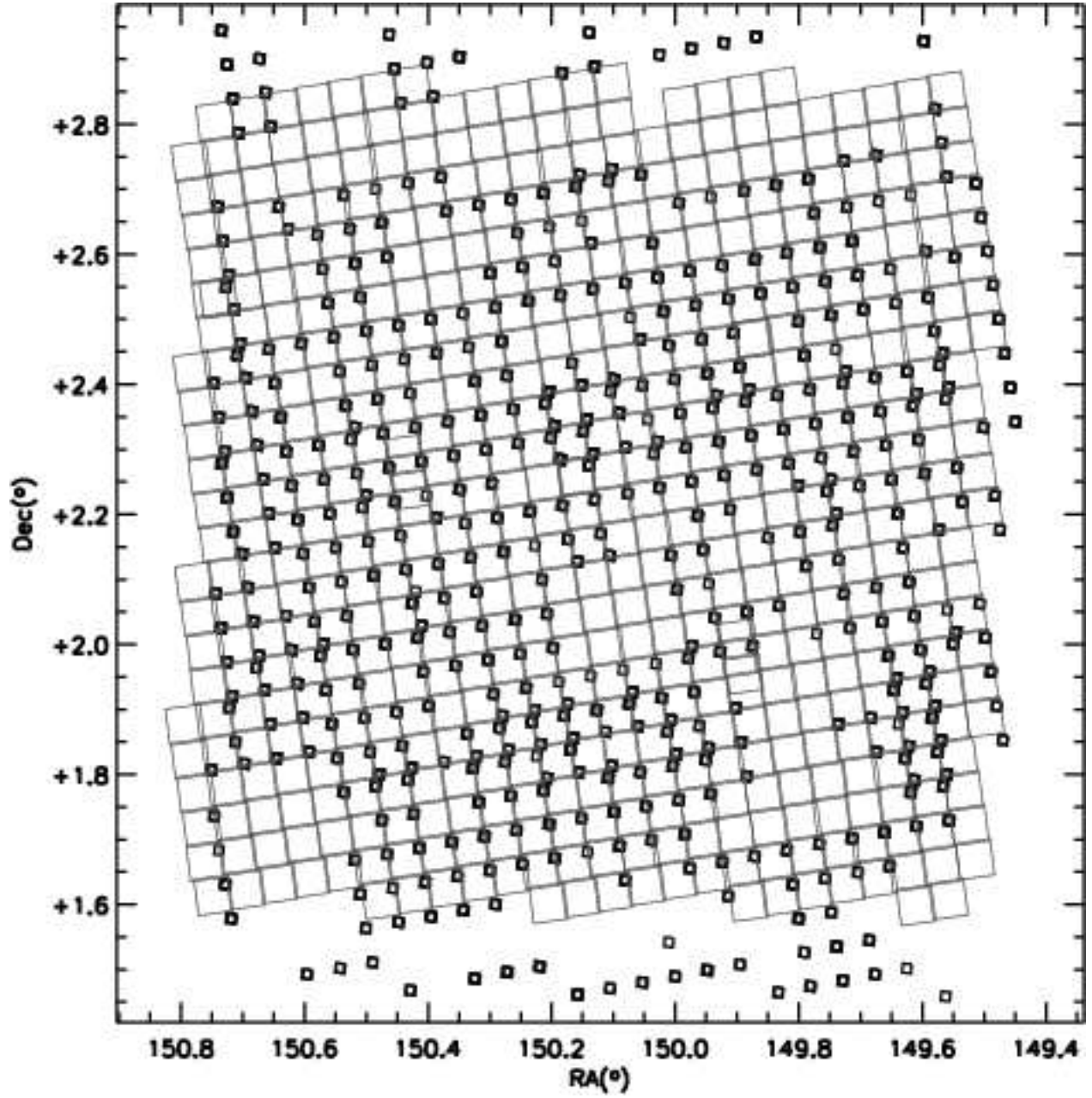


Fig. 2.— The layout of the NICMOS parallels is shown superposed on the ACS pointings. The NICMOS ($1.6\mu\text{m}$) images cover approximately 6% of the ACS area.

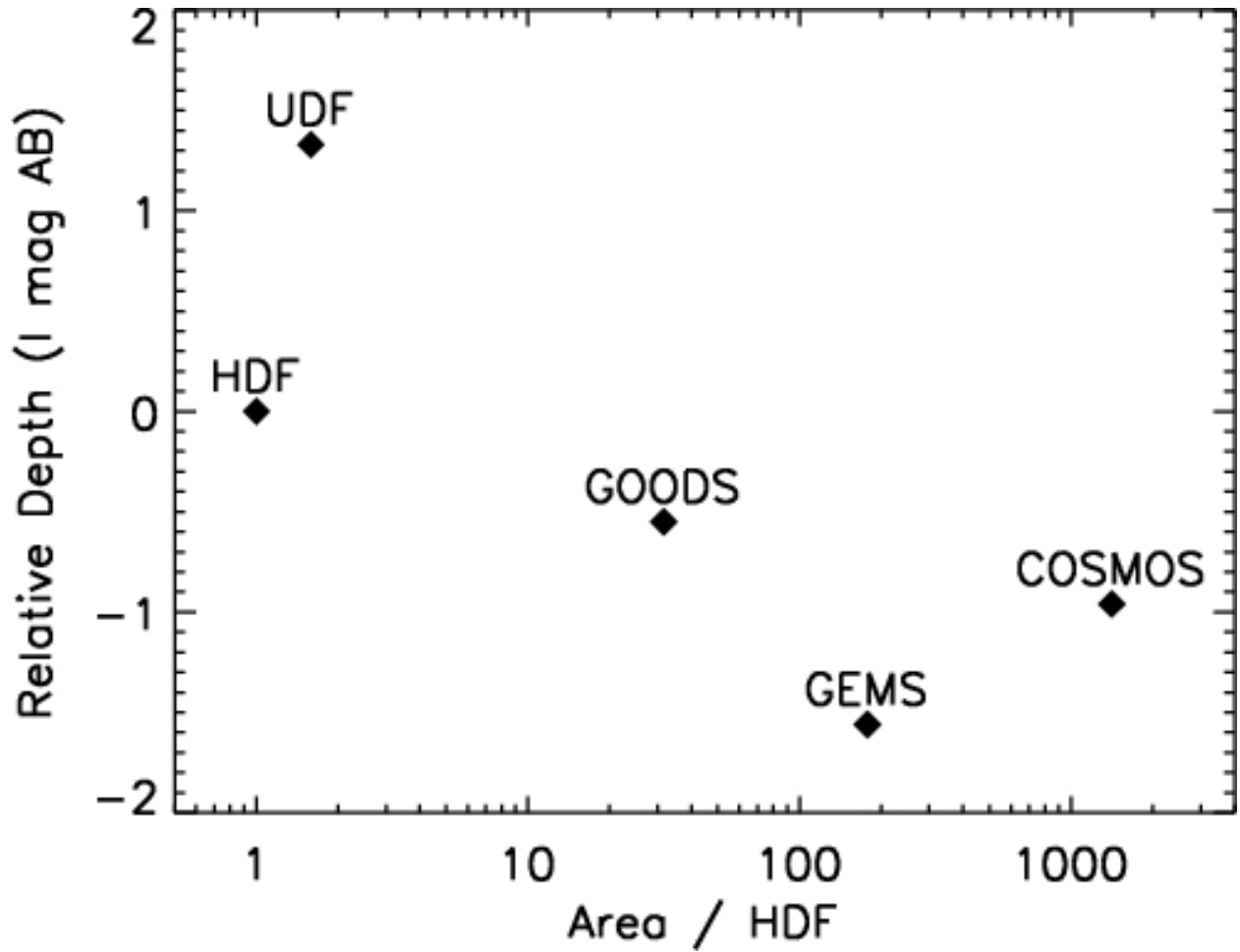


Fig. 3.— Relative field areas and sensitivities of major HST surveys at $\sim 8000\text{\AA}$ compared to the original HDF survey. COSMOS has $9\times$ the area of GEMS (Rix et al. (2004), the next largest survey) with sensitivity just $1.4\times$ less than GOODS (Giavalisco et al. (2004), in 20% the time due to the higher throughput of F814W vs F850LP – GOODS). The relative sensitivities shown here were derived using the instrument exposure time calculators (ETCs for an optimally extracted point source) in order to facilitate equivalent comparisons.

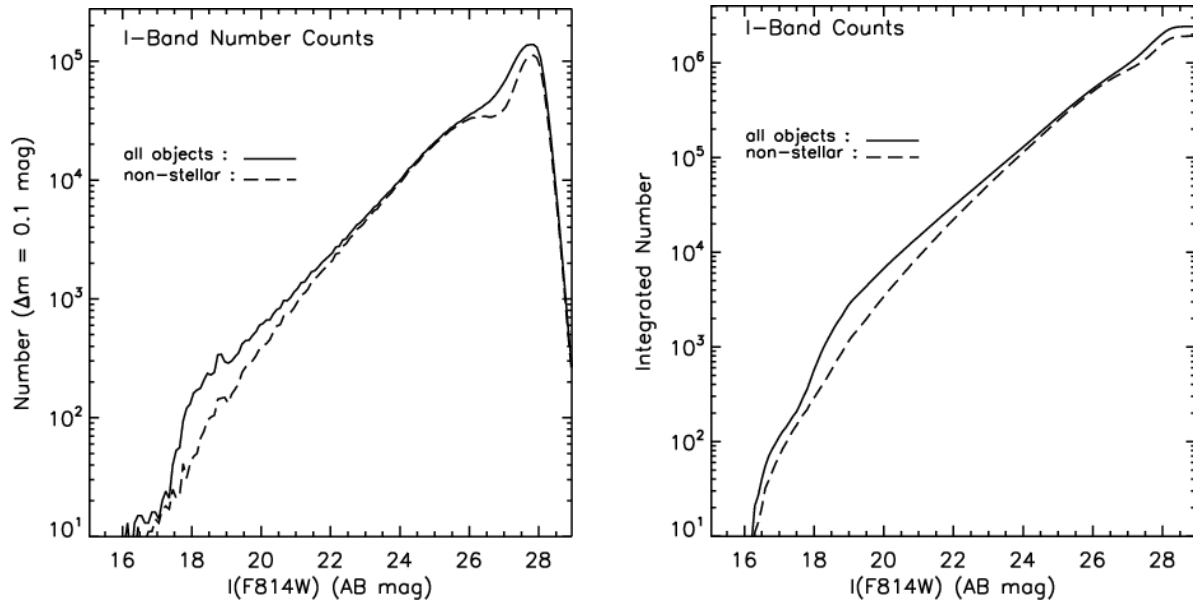


Fig. 4.— Source counts (differential – top panel ; integral – lower panel) for the COSMOS ACS I-band catalog (from SExtractor requiring $> 0.4\sigma$ in at least 4 adjacent pixels and the total isophotal signal-to-noise ratio > 1 .). The number counts for auto-mags are shown for all objects (solid line) and those with ‘stellarity’ < 0.95 (dashed line). The upturn at $I < 27$ mag is the result of low SNR spurious detections. These counts are not corrected for ‘completeness’.

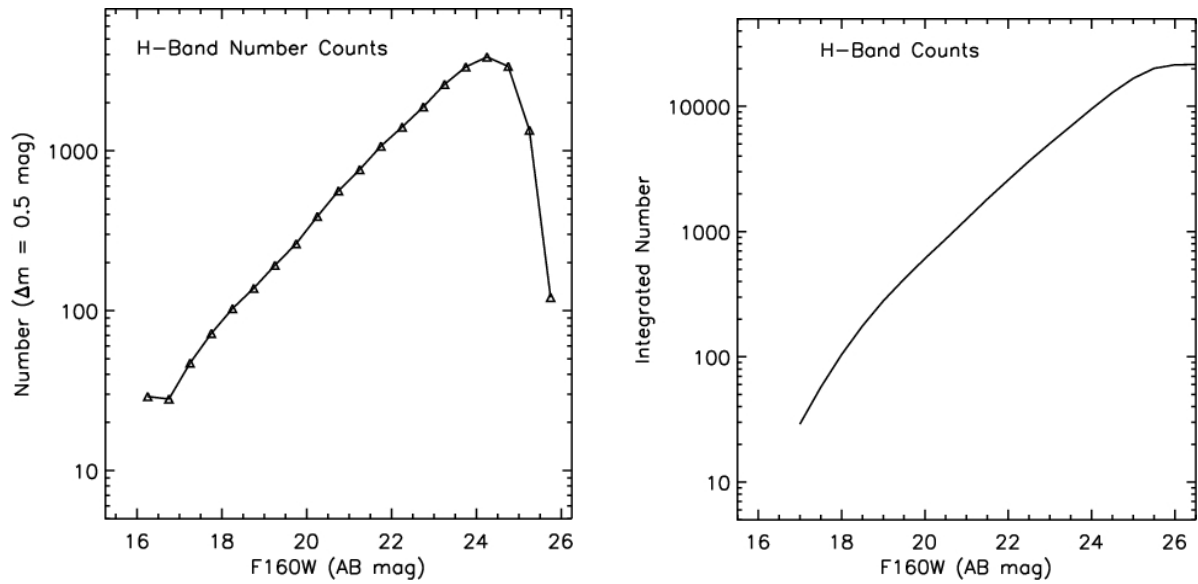


Fig. 5.— Source counts (differential – top panel ; integral – lower panel) for the COSMOS NICMOS H-band catalog (based on SExtractor measurements requiring $> 1.5\sigma$ signal in 9 adjacent pixels). The number counts are for 0.5 mag bins; the total area imaged in NICMOS is $0.099 \square^\circ$. The total number of objects is 21639.

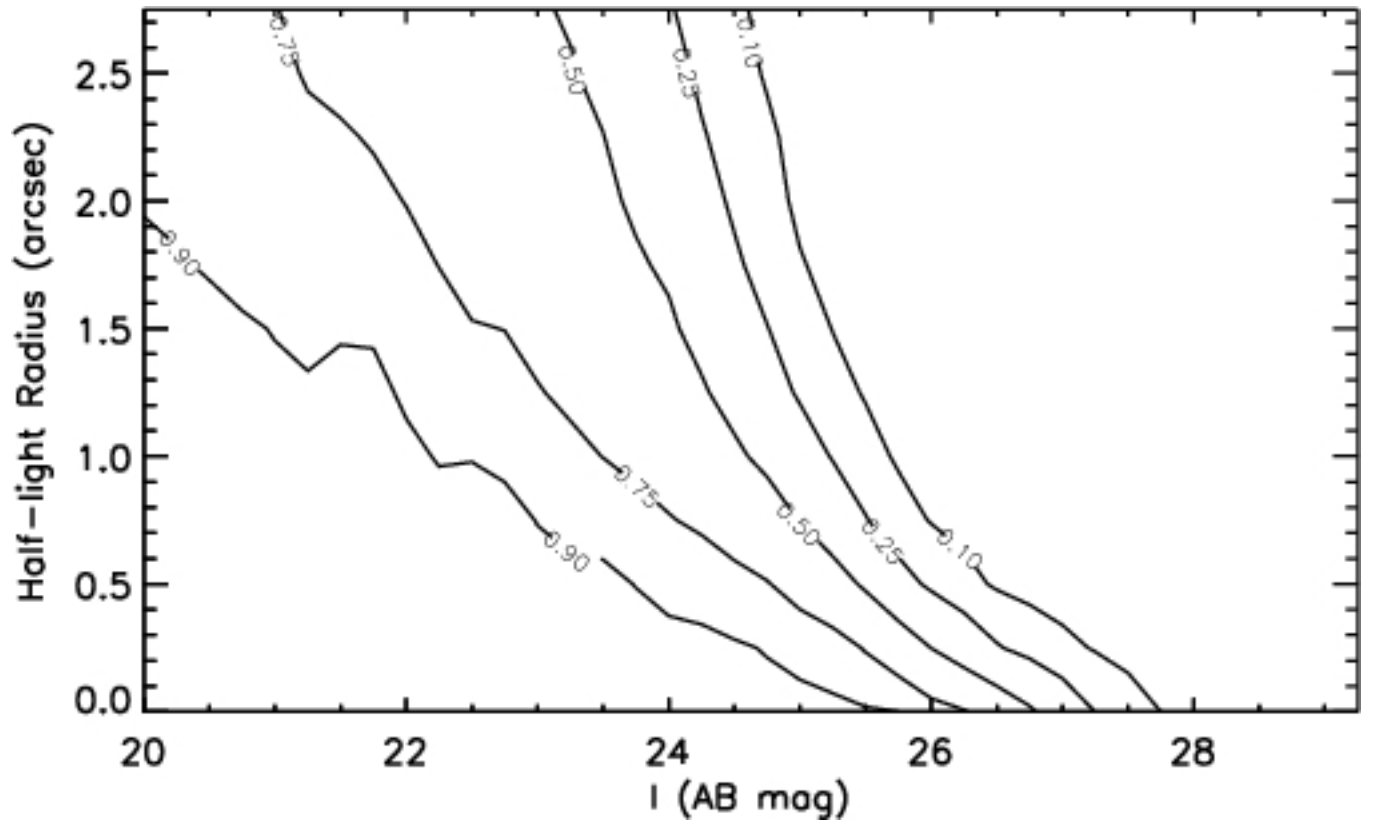


Fig. 6.— Completeness estimates are shown for COSMOS ACS I-band imaging. Contours show the percentage of simulated sources (a 50/50 mix of exponential disks and spheroids) which were recovered by SExtractor as a function of sources total magnitude and half-light radius.